ORIGINAL PAPER

Synthesis and supercapacitance of flower-like Co(OH)$_2$ hierarchical superstructures self-assembled by mesoporous nanobelts

**Changzhou Yuan · Long Yang · Linrui Hou ·
Diankai Li · Laifa Shen · Fang Zhang · Xiaogang Zhang**

Abstract A facile hydrothermal strategy was first proposed to synthesize flower-like Co(OH)$_2$ hierarchical microspheres. Further physical characterizations revealed that the flower-like Co(OH)$_2$ microspherical superstructures were self-assembled by one-dimension nanobelts with rich mesopores. Electrochemical performance of the flower-like Co(OH)$_2$ hierarchical superstructures were investigated by cyclic voltammgoram, galvanostatic charge–discharge and electrochemical impedance spectroscopy in 3 M KOH aqueous electrolyte. Electrochemical data indicated that the flower-like Co(OH)$_2$ superstructures delivered a specific capacitance of 434 F g^{-1} at 10 mA cm^{-2} (about 1.33 A g^{-1}), and even kept it as high as 365 F g^{-1} at about 5.33 A g^{-1}. Furthermore, the SC degradation of about 8% after 1,500 continuous charge–discharge cycles at 5.33 A g^{-1} demonstrates their good electrochemical stability at large current densities.

C. Yuan (✉) · L. Yang · L. Hou · D. Li
Anhui Key Laboratory of Metal Materials and Processing,
School of materials Science and Engineering,
Anhui University of Technology,
Ma'anshan 243002, People's Republic of China
e-mail: ayuancz@163.com

L. Shen · F. Zhang · X. Zhang (✉)
College of Material Science and Engineering,
Nanjing University of Aeronautics and Astronautics,
Nanjing 210016, People's Republic of China
e-mail: azhangxg@163.com

Abbreviations

EC	Selectrochemical capacitors
ECPs	Electrical conducting polymers
SC	Specific capacitance
SSA	Specific surface area
SCE	Saturated calomel electrode
XRD	X-ray diffraction
SEM	Scanning electron microscopy
FESEM	Field-emission scanning electron microscope
SAED	Selected area electron diffraction
TEM	Transmission electron microscope
CV	Cyclic voltammetry
CP	Chronopotentiometry
EIS	Electrochemical impedance spectroscopy

Introduction

According to energy storage mechanism, electrochemical capacitors (ECs) can be classified into two categories: carbon-based electric double-layer capacitors and Faradaic pseudocapacitors based on metal hydroxides/oxides or electrical conducting polymers (ECPs) [1, 2]. As for the electric double-layer capacitors, the energy storage arises from the separation of charges at the interface between the electroactive materials and the electrolyte solution. And for the typical energy storage of pseudocapacitors is contributed by the fast Faradaic reactions, which take place at the electrode materials at characteristic potentials [1]. Considering the low utilization of carbon-based materials [3] and

serious degradation of the ECPs during cycling [4, 5], much effort has been devoted to explore other alternative electrode materials (such as transitional metal oxides or hydroxides) for ECs. Particularly, hydrated RuO_2 has been identified as an excellent material due to its remarkably large specific capacitance (SC) [6, 7]. However, the high cost and toxic nature of the state-of-the-art material have limited its wide applications.

Commonly, cobalt hydroxide, as an active material for battery, was added to enhance the electrochemical performance of nickel hydroxide [8]. Recently, electroactive $Co(OH)_2$ as a good candidate has spurred enormous research in the ECs field, because of its good electrochemical capacitance performance [9–17]. However, the reported SCs for $Co(OH)_2$ are much less than its theoretic SC of 3,650 $F g^{-1}$ [9–15], particularly, at high rates. The next logical strategy is exploring efficient ways to enhance the electrochemical utilization of cobalt hydroxide and enhance its SC at high rates. In terms of pseudocapacitance, it is an interfacial phenomenon related to specific surface area (SSA) and pore structure of electroactive materials and involving the charge transfer through surface Faradaic reactions [2]. Therefore, the electroactive cobalt hydroxide should possess an open and loose structure, which facilitates the electrolyte ions to contact more electroactive sites for fast energy storage at high rates. Moreover, it is still an attractive and significant problem for researchers to explore simple but efficient strategy to prepare cobalt hydroxide with large-scale yield and large SC delivered at high rates.

In this paper, flower-like $Co(OH)_2$ hierarchical microspherical superstructures, to the best of our knowledge, were first self-assembled from the one-dimension mesoporous nanobelts by an interesting biomolecule-assisted hydrothermal strategy. The $Co(OH)_2$ hierarchical superstructures delivered large SCs and good electrochemical stability at high rates. Due to the low cost, simple procedure, large-scale yield and high SC, the flower-like cobalt hydroxide synthesized by this green-chemistry method is a promising material for ECs application.

Experimental

Synthesis and characterization of flower-like $Co(OH)_2$ hierarchical superstructures

All the chemicals used here were of analytical grade. L-Lysine and $CoSO_4 \cdot 6H_2O$ were obtained from Nanjing Chemical Company (Nanjing, China). Saturated calomel electrode (SCE) was manufactured by Leici (Shanghai, China). All aqueous solutions were freshly prepared by using high-purity water (18 MΩ cm resistance) from an Ampeon 1810-B system (Jiangsu, China).

Two grams L-lysine and 1.509 g $CoSO_4 \cdot 6H_2O$ were dissolved in 60 mL high-purity water. And the solution was kept in a Teflon-lined autoclave (80 mL) with a stainless steel shell. After heated to 100 °C, the autoclave was kept at the temperature for 24 h in an oven and then cooled to room temperature naturally. The pink product of the reaction was filtered, washed repeatedly and then dried at 100 °C in vacuum.

The samples were examined by powder X-ray diffraction (XRD; Max 18 XCE, Japan) using a Cu Kα source at a scanning speed of 3°/min over a 2θ range of 10°~80°. Scanning electron microscopy (SEM) images were taken with a field-emission scanning electron microscope (FESEM, JEOL-6300F, 15 kV). Microscope and selected area electron diffraction (SAED) were performed with transmission electron microscope (TEM, FEI, TECNAI-20) and a JEOL-2010 high-resolution (HR) TEM.

Electrochemical tests

The working electrode was prepared by mixing the electroactive material $Co(OH)_2$, acetylene black, and polytetrafluoroethylene in a weight ratio of 5:1.5:0.5. The typical mass of electroactive $Co(OH)_2$ is 7.5 mg. A small amount of water was then added to this mixture to make more homogeneous mixture, which was pressed (about 10^7 Pa) on nickel grid (1 cm^2) for following electrochemical tests by cyclic voltammetry (CV), chronopotentiometry (CP) and electrochemical impedance spectroscopy (EIS) with a frequency response analyzer (Solatron 1255B) interfaced with potential galvanostat (Solatron 1287) controlled by a personal computer. All experiments were carried out in a three-compartment cell with a working electrode, a platinum plate counter electrode (1 cm^2), and a SCE reference electrode. The electrolyte was 3 M KOH aqueous solution.

Results and discussion

Physicochemical characterization

The XRD pattern of the as-synthesized flower-like $Co(OH)_2$ hierarchical superstructures is illustrated in Fig. 1. Six obvious diffraction peaks can be easily identified for the (001), (100), (101), (102), (111), and (103) planes of the hexagonal β-$Co(OH)_2$ crystalline structure, respectively, which is in good agreement with the standard spectrum (Joint Committee on Powder Diffraction Standards file no. 30-0443) with a space group of P-31(164), respectively. No peaks of any other phases or impurities are detected, suggesting high purity of the as-prepared pink $Co(OH)_2$ sample. The formation of β-$Co(OH)_2$ phase was related to the unique biomolecule L-lysine. It is well known that L-
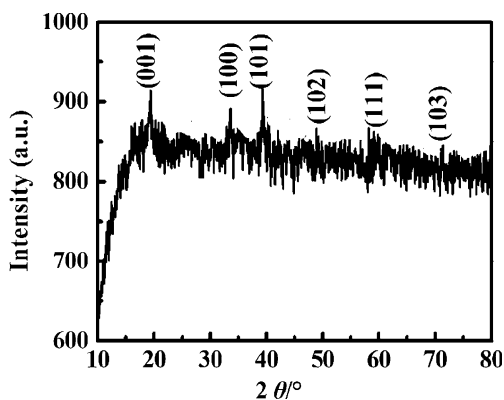
Fig. 1 XRD pattern of the flower-like $Co(OH)_2$ hierarchical microspherical superstructures

lysine is an alkaline amino acid with two amino group and one carboxylic acid group due to the existence of hydrolysis process [11]. And with the increase of temperature, the hydrolysis of the L-lysine can be enhanced greatly and more OH^- ions can be generated accordingly. Consequently, the amino acid solution presents even higher pH, which results in the formation of more and more $Co(OH)_2$ during the hydrothermal process.

Figure 2a–c demonstrate the FESEM images of the Co $(OH)_2$ samples with different magnifications. The as-synthesized $Co(OH)_2$ sample presents a uniform microspherical structure, as seen from Fig. 1a. Furthermore, the magnified FESEM images (Fig. 2b and c) demonstrate that three-dimensional flower-like microspheres with a diameter of 1~2 μm are self-assembled in a radial way by lots of Co $(OH)_2$ nanobelt building blocks. Notably, abundant "V-type" macroporous channels with the size ranged from about 50 to 200 nm present in the $Co(OH)_2$ microspherical superstructures. Particularly, such a macroporous structure, due to its "ion-buffering reservoirs" [18, 19], can offer a robust sustentation of OH^- ions and ensure that sufficient Faradaic reactions take place at high current densities for energy storage. It is worthwhile noting that the as-obtained flower-like $Co(OH)_2$ microspherical superstructures cannot be destroyed and broken into the individual $Co(OH)_2$

Fig. 2 a–c FESEM images with different magnifications for the flower-like $Co(OH)_2$ hierarchical superstructures
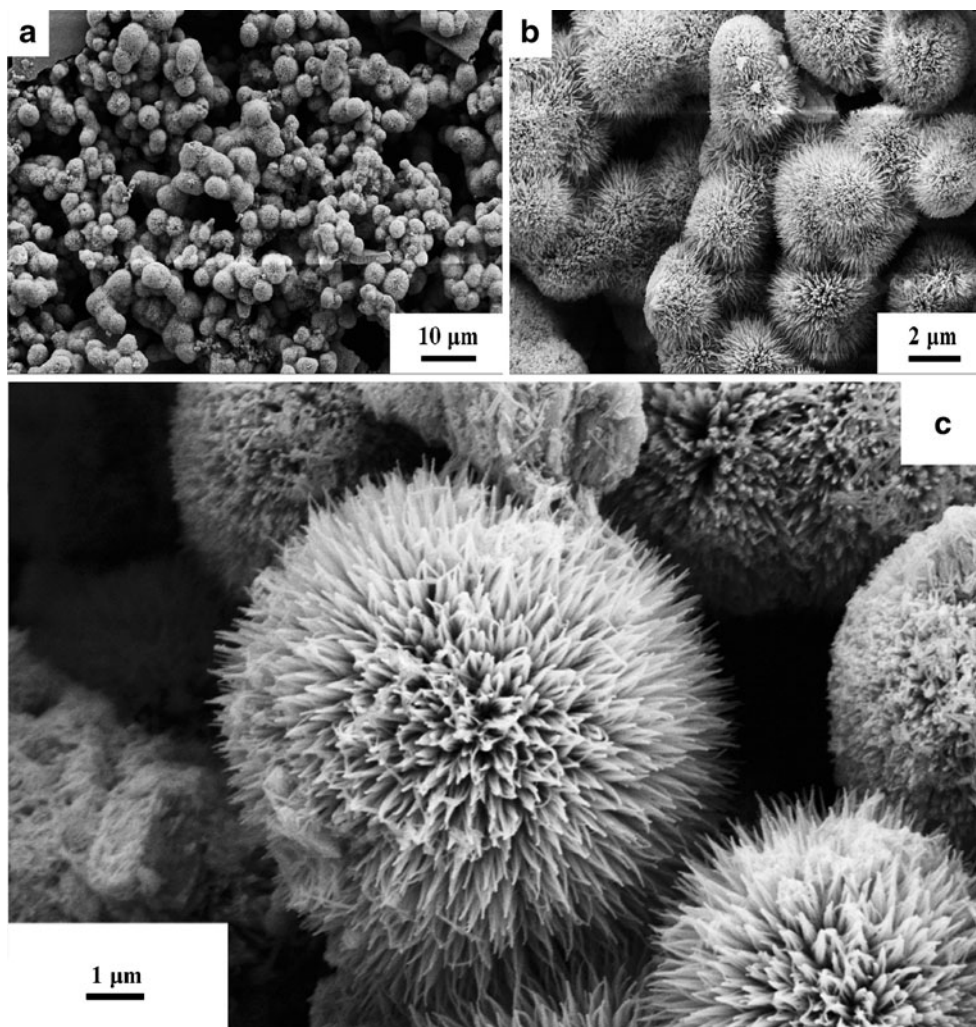
nanobelts even after subjecting long-time ultrasonication. It suggests that the microspherical superstructures are not a random and simple aggregation of one-dimension $Co(OH)_2$ nanobelts but the ordered self-assemble of $Co(OH)_2$ nanobelt building blocks themselves.

In order to demonstrate their microstructures more clearly, the TEM images of flower-like $Co(OH)_2$ microspherical superstructures with different magnifications were shown in Fig. 3a–c. As seen from Fig. 3a, almost all the nanobelts are assembled in a radial form from the center to the surface of microspherical superstructures, which looks like a flower as a whole, although some fragments of the $Co(OH)_2$ nanobelt building blocks can be found. The magnified TEM image (Fig. 2b) demonstrates that the average diameter and length of the nanobelt building blocks can be identified as about 20 and 400 nm, respectively. The high-resolution TEM image (Fig. 3c) clearly presents that the $Co(OH)_2$ nanobelt building blocks own rich mesopores with the average size of about 3 nm. The primary ring pattern of the $Co(OH)_2$ nanobelts can be seen from their

corresponding SEAD pattern (the inset in Fig. 3c), which reveals a typical polycrystalline nature for these nanobelts.

Electrochemical performance of the as-synthesized flower-like $Co(OH)_2$ hierarchical superstructures

For the sake of evaluating the electrochemical characteristics of this unique $Co(OH)_2$ hierarchical superstructures, CV and CP tests were employed to characterize their electrochemical capacitance. CV curves of the flower-like $Co(OH)_2$ hierarchical superstructures are presented in Fig. 4a. Obviously, two pairs of redox peaks (designated as O/R and O'/R'), at various scan rates as indicated, demonstrate their typical Faradaic pseudocapacitive characteristics [9–17], as presented by the following two equations:

$$Co(OH)_2 + OH^- \rightleftharpoons CoOOH + H_2O + e^- \tag{1}$$

$$CoOOH + OH^- \rightleftharpoons CoO_2 + H_2O + e^- \tag{2}$$
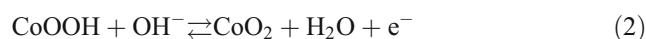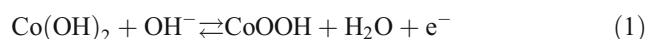
Fig. 3 TEM images (**a**, **b**, and **c**) with different magnifications and SAED pattern (*the inset*) of the flower-like $Co(OH)_2$ hierarchical superstructures
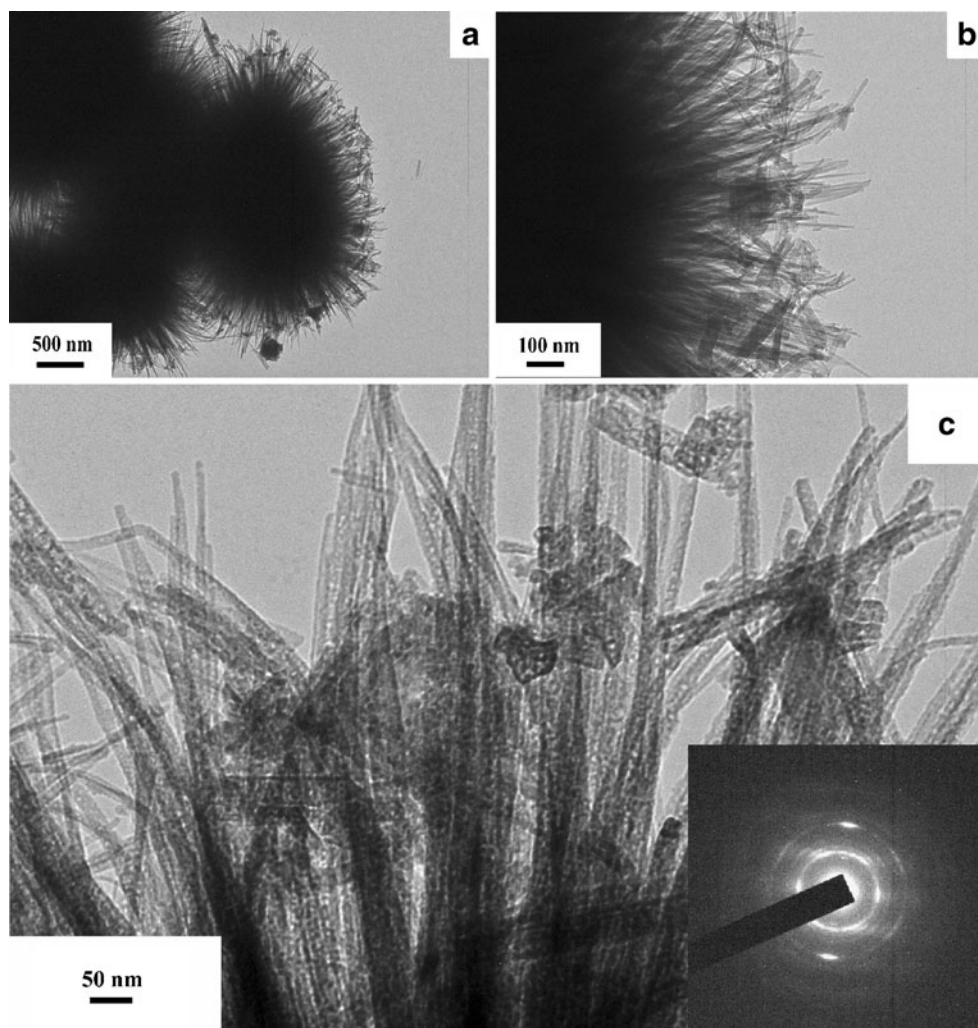
Specifically, the peak O is related to the oxidation of Co(II) to Co(III)OOH, and the peak R is for the reverse process, as shown in Eq. 1. The peak O' is due to the oxidation of Co(III)OOH to Co(IV)O$_2$, and the peak R' is therefore attributed to the reduction of Co(IV)O$_2$ to Co(III)OOH, as demonstrated in Eq. 2. In addition, electrochemical response currents of these CV curves on the positive sweeps are nearly mirror-image symmetric to their corresponding counterparts on the negative sweeps with respect to the zero-current line. The current subsequently increases while the CV shape almost keeps the same with the increase of the scan rate, which shows good electrochemical capacitance of the as-synthesized Co(OH)$_2$ hierarchical superstructures.

The typical CP plots of the flower-like Co(OH)$_2$ hierarchical superstructures at various current densities are demonstrated in Fig. 4b. A symmetric shape during the charge/discharge processes is observed, suggesting their good supercapacitive performance. And some slopes in the charge and discharge plot can be clearly observed, which is corresponding to typical two-electron Faradaic reaction among different valences of Co species, that is, Co^{4+}/Co^{3+} and Co^{3+}/Co^{2+}, which is in good agreement with the analysis about the CV curves in Fig. 4a. The SCs of the flower-like Co(OH)$_2$ hierarchical superstructures were calculated from the CP curves according to the following Eq. 3:

$$C = \frac{It}{m\Delta V} \tag{3}$$

where C, I, t, m, and ΔV are the SC (F g^{-1}) of the Co(OH)$_2$ electrode, the discharging current density (A cm^{-2}), the discharging time (s), the mass of the electroactive Co(OH)$_2$ (g), and the discharging potential range (V), respectively. Another important parameter, Coulombic efficiency (η), can be evaluated from Eq. 4, where t_D and t_C are the discharging time and charging time, respectively.

$$\eta = \frac{t_D}{t_C} \times 100\% \tag{4}$$

The SCs and coulombic efficiencies of the flower-like hierarchical superstructures at various current densities can be calculated based on the charge–discharge curves in Fig. 4b and the typical data are collected in Fig. 4c. Impressively, a SC of 434 F g^{-1} can be achieved by the flower-like Co(OH)$_2$ microspherical superstructures at 10 mA cm^{-2} (about 1.33 A g^{-1}), and 365 F g^{-1} even at 40 mA cm^{-2} (about 5.33 A g^{-1}), which reveals its great ability to deliver large SC at high rates. These data means that flower-like Co(OH)$_2$ hierarchical superstructures with rich hierarchical porosity

Fig. 4 CV curves (**a**), CP plots (**b**), and SCs as a function of current densities (**c**) of the flower-like Co(OH)$_2$ hierarchical superstructures
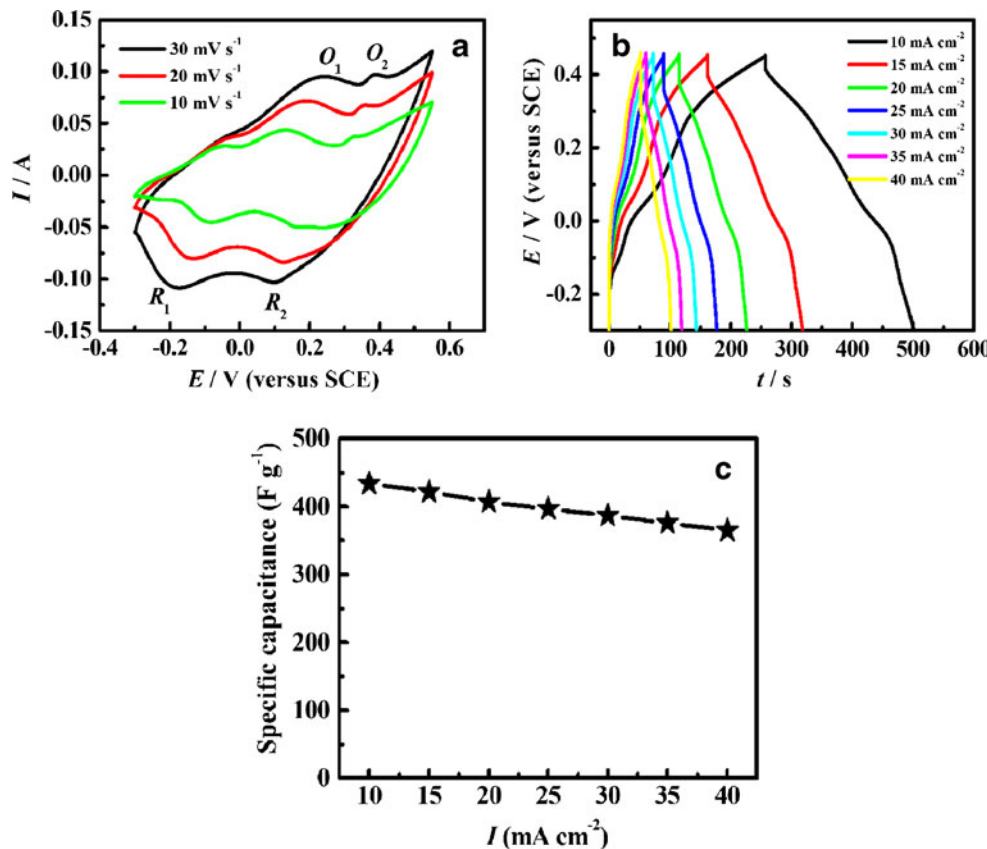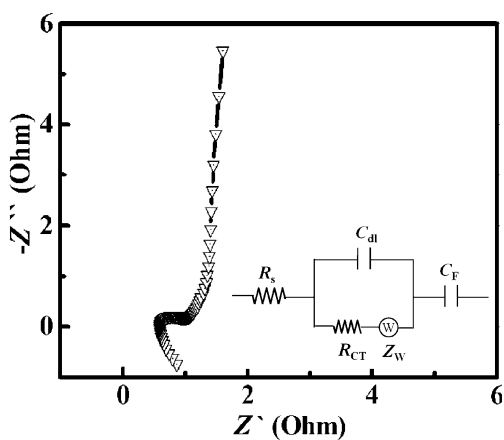
Fig. 5 EIS plot and fitting equivalent-circuit model (*the inset*) of the flower-like $Co(OH)_2$ hierarchical superstructures at 0.2 V

Table 1 The values of the equivalent circuit elements for the flower-like $Co(OH)_2$ hierarchical superstructures

R_s (Ω cm^{-1})	0.62
C_{dl} (F g^{-1})	22.23
R_{CT} (Ω cm^{-1})	0.39
Z_W (Ω S$^{-1/2}$)	0.45
C_F (F g^{-1})	383
Errors (%)	0.991

can serve as a good electroactive material for ECs, due to their ability to provide promising energy density and maintain it at high charge/discharge rates. These rich and hierarchical diffusion channels can reduce the diffusion lengths for electrolyte ions and ensure enough electrolyte ions to rapidly contact much more electroactive sites of the mesoporous $Co(OH)_2$ nanobelts for efficient energy storage, which guarantees high electrochemical utilization and higher-rate charge/discharge performance of the unique electrodes. In addition, the coulombic efficiencies at different current densities are all more than 96%, and even up to 100% when the current densities are not less than 20 mA cm^{-2}, which reveals the good electrochemical reversibility of the flower-like $Co(OH)_2$ microspherical superstructures.

The electrochemical process mentioned above can be further verified by the EIS measurement. Figure 5 depicts the typical Nyquist plot with a frequency loop from 100 kHz to 0.01 Hz using a perturbation amplitude of 5 mV. Of note, several features must be described here. Firstly, the high-frequency intersection of the plots at the real axis represents the internal resistance (R_s) [20], which commonly includes the following three aspects: the resistance of the KOH aqueous solution, the intrinsic resistance of the electroactive material itself and the contact resistance at the interfaces between electroactive materials and current collector. Secondly, in the high-frequency range, a little semicircle, resulting from the parallel combination of double-layer capacitance (C_{dl}) and charge transfer resistance (R_{CT}) at the electroactive material–electrolyte interface, reveals the small R_{CT} and C_{dl}, respectively. Thirdly, in the intermediate-frequency region, the 45° line can be seen, suggesting the existence of finite-length Warburg resistance (Z_w) in the ion diffusion into the porous structure of the electrode. Finally, in the low frequency, the linear region leans more towards imaginary axis, indicating good supercapacitive behavior (C_F) of the

as-prepared hierarchical microspherical superstructures. The fitting equivalent-circuit model is shown in the inset in Fig. 5. And the best-fit values of the equivalent-circuit elements are listed in Table 1.

According to the data presented in Table 1, the C_{dl} and C_F of the flower-like $Co(OH)_2$ hierarchical superstructures is as large as 0.1667 and 2.8725 F, respectively, that is, about 22.23 and 383 Fg^{-1}, respectively. It means that the main component of the measured SC is produced from the pseudocapacitive surface redox process, rather than the simple separation of charges at the interfaces between the electroactive materials and the electrolyte solution. According to the Brunauer–Emmett–Teller SSA of an average value of 20 μF cm^{-2}, the electric double-layered capacitance of about 20 Fg^{-1} can be calculated, and the electrochemical SSA of the flower-like $Co(OH)_2$ micro-spherical superstructures is estimated as about 111 m^2 g^{-1}. Accordingly, the Faradaic psedocapacitance is calculated as about 345 μF cm^{-2}, suggesting their high electrochemical utilization. Moreover, the Warburg resistance is as little as about 0.45 ΩS$^{-1/2}$, which should be related to their favorable hierarchical porous structures. Furthermore, the charge transfer resistance and the internal resistance are just 0.39 and 0.62 Ωcm^{-1}, respectively. Out of question, the little R_{CT}, R_s, and Z_W facilitate the electrolyte ions and electrons to easily contact the electroactive $Co(OH)_2$ mesoporous nanobelt building blocks at high rates and ensure that sufficient Faradaic reactions can take place at
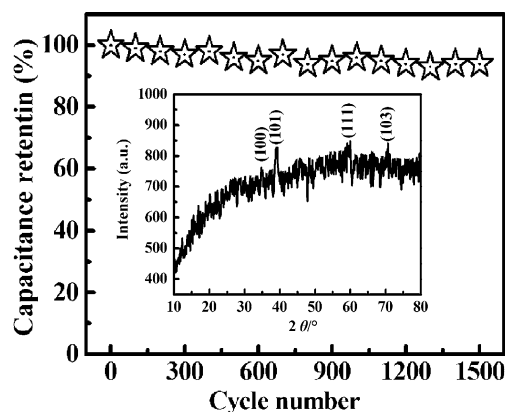
Fig. 6 Cycling performance of the flower-like $Co(OH)_2$ hierarchical superstructures and the *inset* for their XRD pattern after 1,500 continuous charge–discharge cycles

high current densities for energy storage, which is favorable for the good power property of the flower-like $Co(OH)_2$ hierarchical superstructures, as mentioned above.

The cycle performance of any electroactive material is one of the most significant parameters for its practical applications. The cycle life of the flower-like $Co(OH)_2$ microspherical hierarchical superstructures was carried out at a constant current density of 40 mA cm^{-2}. After continuous 1,500 charge–discharge cycles, the SC decreases from 365 to 336 F g^{-1}. The SC decrease after cycling at such large current density of about 5.33 A g^{-1} should be related to some chemical degradation of the $Co(OH)_2$ superstructures. It can be evident from their XRD pattern (the inset in Fig. 6), in which the diffraction peaks ascribed to the (001) and (102) planes disappear although the (100), (101), (111), and (103) planes of the β-$Co(OH)_2$ phase still can be found after 1,500 continuous cycles. A SC degradation of about 8% (Fig. 6) still reveals a good electrochemical stability of the unique flower-like $Co(OH)_2$ hierarchical superstructures at large current densities.

Conclusions

In summary, we first propose an efficient synthetic strategy to synthesize the flower-like $Co(OH)_2$ hierarchical microspherical superstructures. The unique superstructures were self-assembled by one-dimension mesoporous $Co(OH)_2$ nanobelts. Electrochemical data demonstrated that the flower-like $Co(OH)_2$ hierarchical superstructures delivered a specific capacitance of 434 F g^{-1} at about 1.33 A g^{-1}, and even kept it as high as 365 F g^{-1} at about 5.33 A g^{-1}. The specific capacitance retention remained at about 92% after 1,500 continuous charge–discharge cycles at about 5.33 A g^{-1}, which reveals their good electrochemical stability at high rates. Moreover, the preparation we described here is much simple and cost-effective for large-scale production of the flower-like $Co(OH)_2$ hierarchical microspherical superstructures with good electrochemical performance for ECs applications.

References

1. Conway BE (1999) Electrochemical supercapacitors, scientific fundaments and technological applications. Kluwer Academic/Plenum, New York
2. Yuan CZ, Gao B, Shen LF, Yang SD, Hao L, Lu XJ, Zhang F, Zhang LJ, Zhang XG (2011) Nanoscale 3:529–545
3. Frackowiak E, Delpeux S, Jurewicz K, Szostak K, Cazorla-Amoro D, Beguin F (2002) Chem Phys Lett 361:35–41
4. Burke A (2000) J Power Sources 91:37–50
5. Chen L, Yuan CZ, Dou H, Gao B, Chen SY, Zhang XG (2009) Electrochim Acta 54:2335–2431
6. Sugimoto W, Iwata H, Yasunaga Y, Murakami Y, Takasu Y (2003) Angew Chem Int Ed 42:4092–4096
7. Yuan CZ, Chen L, Gao B, Su LH, Zhang XG (2009) J Mater Chem 19:246–252
8. Falk SU, Salkind AJ (1969) Alkaline Storage Batteries. Wiley, New York, p 54
9. Cao L, Xu F, Liang YY, Li HL (2004) Adv Mater 16:1853–1857
10. Liang YY, Cao L, Kong LB, Li HL (2004) J Power Sources 136:197–200
11. Yuan CZ, Zhang XG, Hou LR, Shen LF, Li DK, Zhang F, Fan CG, Li JM (2010) J Mater Chem 20:10809–10816
12. Hu ZA, Xie YL, Wang YX, Xie LJ, Fu GR, Jin XQ, Zhang ZY, Yang YY, Wu HY (2009) J Phys Chem C 113:12502–12508
13. Yuan CZ, Zhang XG, Gao B, Li J (2007) Mater Chem Phys 101:148–152
14. Zhao T, Jiang H, Ma J (2011) J Power Sources 196:860–864
15. Wu CM, Fan CY, Sun IW, Tsai WT, Chang JK (2011) J Power Sources 196:7828–7834
16. Chen S, Zhu J, Wang X (2010) J Phys Chem C 114:11829–11834
17. Zhou WJ, Zhang J, Xue Tong, Zhao DD, Li HL (2008) J Mater Chem 18:905–910
18. Wang DW, Li F, Liu M, Lu GQ, Cheng HM (2008) Angew Chem Int Ed 47:373–376
19. Yuan CZ, Zhang XG, Su LH, Gao B, Shen LF (2009) J Mater Chem 19:5772–5777
20. Yuan CZ, Zhang XG, Wu QF, Gao B (2006) Solid State Ionics 177:1237–1242